Comparison of the Critical Mass Flow Rates for Two Serpentine Designs of the Photovoltaic Solar Thermal Collector

Sakhr M. Sultan*, C.P. Tso and M.N. Ervina Efzan

Faculty of Engineering and Technology, Multimedia University, Jalan Ayer Keroh Lama, 75450, Melaka, Malaysia

Abstract: A recent analysis on the photovoltaic (PV) cell efficiency for the photovoltaic solar thermal collector (PVT), cooled by forced fluid flow, revealed that there is, in general, a critical mass flow rate that corresponds to the maximum PV cell efficiency for a PVT. The derived new equations are applicable for laminar and transition or turbulent flow regimes and could yield directly the critical mass flow rate as compared with existing methods that use repeated computational trials. To demonstrate further the generality of the method, this paper reports results on comparing the critical mass flow rates for two serpentine designs with different technical details, namely Design A and Design B, using the new equations. It is shown that Design A and Design B have critical mass flow rates of 0.041 and 0.014 kg/s, respectively. The corresponding Reynolds numbers are 4078 and 2785 for Design A and Design B, respectively. It is shown that the critical mass flow rate is different from one design to another. The importance of the critical mass flow rate is summarized.

Keywords: Solar energy, Photovoltaic solar thermal collector, Surpentine collector design, Critical mass flow rate, Pumping requirement, Photovoltaic cell efficiency.

1. INTRODUCTION

The grouping of photovoltaic (PV) together with solar thermal collector technologies leads to the formation of photovoltaic solar thermal collectors (PVT) [1]. The major advantages of a PVT are the generation of both electricity and heat. Generally, a PVT is divided into two types; a water or air-based photovoltaic solar thermal collector. The main components of a water-based PVT are a PV and a solar collector that circulates the cooling water with a pump [2-3]. An insulation material is usually incorporated to reduce heat loss from the system, as shown in Fig. (**1**). A PVT utilizes the collector for absorbing and transferring heat to the water, which can then be utilized, and more importantly, the heat withdrawn from the PV will enhance the PV performance [4-6].

Garg and Agarwal [8] studied a closed-loop PVT that operated over a day with varying solar radiation and ambient temperature. Then, using simulations, the time-averaged daily cell efficiency was plotted, at various flow rates, from which it was found that there was a daily optimum flow rate identifiable by observation. The pump was operated based on an on/off switch and depended on the changes of the solar radiation and ambient temperature. At the optimum efficiency, the coolant mass flow rate called the critical mass flow rate, $\dot{m}$, was 0.03 kg/s, when the maximum PV efficiency was 8.1 %.

*Address correspondence to this author at the Faculty of Engineering and Technology, Multimedia University, Jalan Ayer Keroh Lama, 75450, Melaka, Malaysia; E-mail: mas2007_eng@yahoo.com

The experimental measurements showed that the electrical and thermal efficiencies of the proposed design were 0.7 % higher than the conventional PV efficiency and 44.37 %, respectively. It was concluded that the overall efficiency of the glass to glass PVT was improved. The evaluation of the electrical performance of a water-based PVT was carried out [9]. The artificial neural networks (ANNs) for machine learning and neuro-fuzzy were applied for improving the simulation models of a PVT. The parameters such as solar radiation, mass flow rate & inlet temperature were considered as the input variables in the proposed model. Experimental measurements were carried out for a novel PVT design. A good agreement was achieved between the proposed model results and the experimental measurements. It was concluded that the proposed method can solve the problem associated with the experimental setup such as time and cost. A new PVT liquid type was proposed [10]. A phase change material (PCM) tank was integrated into PV's backside. As a result, the PV performance could be improved due to PV's temperature control during the process of the phase change.

The effect of dispersing copper (Cu) and alumina (Al_2O_3) nanoparticles in pure water on the performances of a PVT was investigated [11]. The numerical model was developed which is derived from the energy balance equations. Experimental measurement was conducted and compared with the analytical results and they were in good agreement. Results showed that Cu-water nanofluid provided a better PVT performance as compared with Al2O3. To overcome the drawback of

E-ISSN: 2409-5826/20

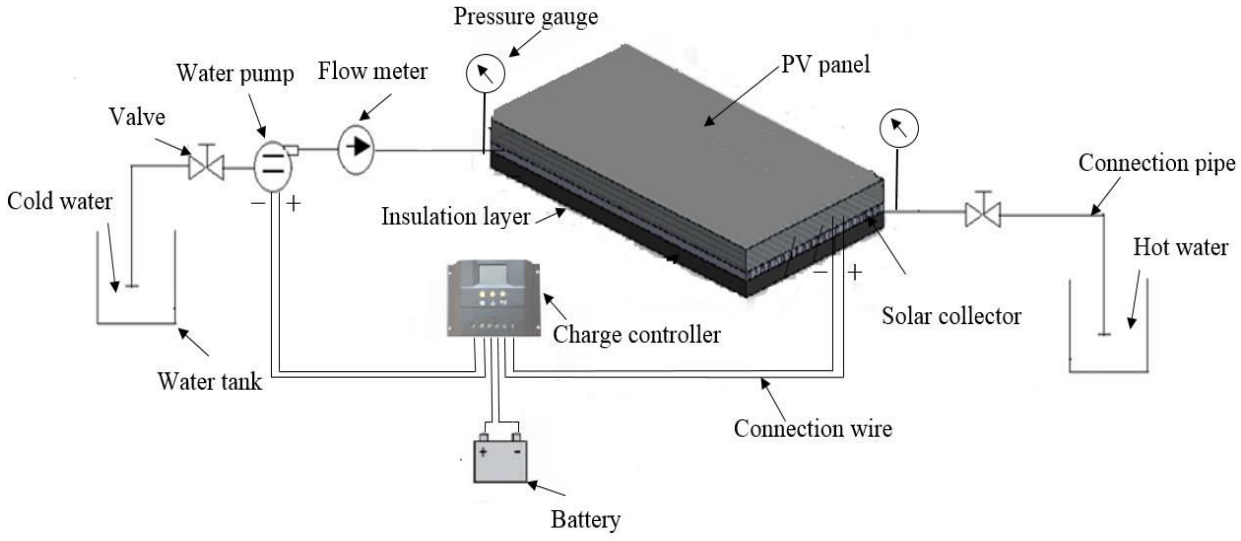

Figure 1: Line diagram of a PVT [7].

low PVT output temperature, an innovative PVT was proposed [12]. A two-dimensional steady model was developed and validated with experiments. A comparative study was performed and indicated that the proposed PVT had lower electrical performance but can produce relatively high thermal efficiency.

The annual energy, exergy gain, and CO_2 mitigation were also elaborated. Erkata Yandri (2019) proposed methods for the development of polymeric PVT in indoor experiment testing. He developed a PVT with a collector made of a polymethyl-methacrylate (PMMA). By performing experiments, he tested the developed PVT by varying the irradiance, mass flow rate, and inlet water temperature. The results showed that PMMA as a collector provides a good PV cooling effect [13].

The design of an innovative glazed water-based PVT and the development of a detailed mathematical model for the prediction of its electrical and thermal generation were carried out [14]. The work presented a covered PVT design, utilizing thin-film PV and a flat plate with a roll-bond absorber. Finally, considerations about the daily and annual energy yield of the proposed PVT as compared to a standard PV were also elaborated. They concluded that more work must be concentrated on the performance of PVT in summer in order to understand the regeneration effect of a-Si/lc-Si due to high temperatures.

Theoretical and experimental studies were conducted on a new PVT configuration [15]. The new PVT design was tube and sheet type which has the advantages of having a better heat extraction and low cost compared to other PVT configurations. Results showed that the electrical and thermal efficiencies were 11.12 % and 54.51 %, respectively.

Mathematical and experimental investigations of five asymmetric PVT with a flat plate receiver connected in series were studied [16]. The performance evaluation in terms of energy and exergy thermal production under different operating conditions was discussed. The developed mathematical model combined optical, flow, and the first and second law efficiency determination, and validated with the experiments. The performance of the PVT was analyzed in terms of absorber temperature, thermal and exergy efficiency. The experimental data proved that solar collectors that were connected in series work more efficiently throughout the year as they were able to harvest about 2.2 kW of useful energy gain in summer, 2.8 kW in spring, and 2.6 kW in autumn.

The development of the numerical characteristic equation for N identical fully covered PVT-CPC integrated solar distillation system was carried out [17]. The disadvantages of the partially covered PVT are low thermal performance, higher maintenance cost, and high fabrication cost. The analytical characteristic equation development consisted of deriving the energy balance equations for different PVT components. The proposed N-PVT-CPC integrated active solar distillation system results were compared with fully covered N identical PVT-FPC integrated solar distillation system and conventional N identical FPC active solar distillation system.

An experimental set up of fully covered CPVT was designed and fabricated to enhance its performance [18]. The system was mounted on the rooftop. A semi-transparent PV was used to cover the CPVT. A clear sky day condition was taken into consideration and two cases were studied on the basis of the rotation of the receiver, according to the movement of the sun, to analyze the annual behavior of the present system. Case (i): fixed position and Case (ii): manual maximum power point tracking technique (M-MPPT). The manual tracking was adopted for 3 times a day in a three hours interval (09.00–12.00–15.00 h). Consecutive days were chosen for both cases in each month throughout the year. It was observed that there was a good agreement between the theoretical analysis and the experimental data taken.

The operating parameters of N-fully covered semi-transparent PVT-CPC have been analyzed for a constant collection temperature mode [19]. The analysis was carried out based on the basic energy balance equations for the PV, absorber plate, flowing fluid, concentrator, and others. Analytical modeling was carried out using MATLAB R2015a. The proposed system performance was compared with the performance of PVT-FPC, FPC-CPC, and FPC. It was shown that the overall exergy of N-fully covered semi-transparent PVT-CPC decreased with the increase of the constant collection temperature. Therefore, the overall thermal energy of the N-fully covered semi-transparent PVT-CPC system increased with the decrease of the packing factor.

The development and the validation of a first-order dynamic model with experimental data for a PVT were presented [20]. The model used the analytical solution of the energy balance equation, to predict the mean temperature of the collector via an iteration process. The parameters of the PVT such as the efficiency factor and the overall heat loss coefficient were predicted for every step, while the optical efficiency of the PVT was analytically calculated using the optics principal laws. The analytical results were in good agreement with experimental measurements. The outlet water temperature collector was predicted to be 0.66 % for stable weather conditions and to be 4.22 % for very transient conditions with sporadic showers. Lastly, by considering the heat inertia of the absorber on energy balance equations of the collector, a good contribution to the accuracy of the model can be achieved, contrary to the steady-state model.

An energy performance of ETFE (ethylene tetrafluoroethylene) cushion roof integrated with PVT (CIPVT) was carried out [21]. An experimental set-up composed of an amorphous silicon PV module and three-layer ETFE cushion roof was developed to examine the system performance from 10:00 a.m. to 5:00 p.m. under ambient temperature of 9 ^{o}C and 39 ^{o}C in December 2014 and August 2015, respectively. The experimental measurements showed that the developed CIPVT was operating steadily. A low winter solar radiation to strong summer solar radiation was selected to study the performance of CIPVT. It was found that the average total and net electricity were 54.5Wh and 42.9 Wh, respectively. A PVT was fabricated and examined under outdoor operating conditions [22]. The mathematical model, correlations for Nusselt number for PV, and transpired plate were derived using a computational fluid dynamics (CFD) model. The experimental measurement and simulated values were in good agreement, with the maximum relative root mean square percent deviation (RMSE) of 9.13 % and minimum correlation coefficient (R-squared) of 0.92.

A low concentrating PV and PVT were fabricated and examined for a given spring climatic condition of the Tunisian Saharan city, Tozeur [23]. The system was an asymmetric compound parabolic PV concentrator. The comparison confirmed that the electrical performance can be improved. The experimental measurements were compared with the output of the CFD model and they were in good agreement. The influence of CPC reflectors on the PV efficiency was presented [24]. The effect of the distribution of the flux was measured on a real scale collector on an outdoor test stand. The inclination angle modifier (IAM) of the PV performance was measured for three concentrations, aiming to homogenize the distribution of the flux in the cell of the PV. The experiment measurements showed that the PV performance drops from 15 % at standard test conditions to between 9 % and 11 %.

The main drawbacks of the development of PVT are the unavailability of an internationally recognised standard testing methodology or a procedure to compare various PVTs with each other and with conventional alternatives [25]. A complete procedure to characterise, simulate and assess concentrating PVT was proposed and demonstrated in a specific case study. By using the proposed testing procedure, the PVT factors were determined by experiments. These were used in a validated simulation prototype that predicts the outputs of the PVT at various geographical positions. Moreover, the method included a comparison of the performance of the PVT with conventional solar

collectors and PV modules that were operating side-by-side. The experiments showed that the PVT electrical performance was 6.4 % while the optical efficiency was 0.45.

A performance model that allows the estimation of PVT was presented which can be applied for PVT and CPVT [26]. The model was built based on energy balance, heat transfer, and the dependence of the PV performance on the temperature of the PVT. Like the quasi dynamic model for solar thermal collector, linear parameterizations of both thermal and electrical power outputs were derived. The corresponding linear coefficients were found from multi-linear regression on solely standard measurement data. Good agreement was achieved from empirically determined absorber coefficients with expectations from well-known factors.

A proposed model for a V-trough CPVT was theoretically and experimentally validated [27]. The results revealed that the proposed design gave improved electrical performance. Also, it was shown that the V-trough could be made of durable stainless steel while still giving a 25% increase in solar radiation over a typical year.

A cycloidal transmissive Fresnel solar concentrator design that can offer a certain width focal line was presented [28]. Based on the principle of optical refraction, each wedge-shaped component of Fresnel lens dimensions was calculated. An optical simulation was done to get the concentrator optical efficiency for different axial incidence angles and tracking errors. It was found that about 80% of the solar radiation can be collected by the absorber when the tracking error was within 0.7o. Therefore, it has no influence on the receiving rate when the incidence axial angle is within 10o. The concentrating PVT integrated with transmissive Fresnel solar concentrator was designed. An experimental work for cylindrical Fresnel concentrating PVT was conducted under the real sky. The distribution of the temperature on the receiver, thermal energy, and electrical energy outputs of concentrating PVT were the main parameters for testing. The experimental measurements in clear weather showed that the electrical and thermal performances were 18 and 45 %, respectively.

A building-integrated CPVT was designed, fabricated, and experimentally investigated. Comparative performance with a non-concentration system was shown to analyze the differential outputs [29]. The concentration contained double side reflective strips. The thermal output of the building-integrated CPVT was almost double that of the non-concentration system and the electrical performance was more than 4.5 times in the case of the concentrating module.

A new design of a PVT was proposed and investigated [30]. A silicon monocrystalline PV was integrated with proper reflectors used to increase insolation in conjunction with a closed-loop cooling facility to extract the PV heat effectively. The collected heat from the PV is used to heat the water flow before entering four vacuum tube solar water heaters placed on both sides of the PV. Performance evaluation was compared to a similar bare PV module. It was shown that there was a significant improvement in the thermal and electrical energy outputs.

The integration of both mediums with the conventional PVT was presented [31]. For electricity generation, the main elements fabricated in the PVT were two transparent PV connected in parallel, with a double pass flat-plate air type heater, copper tubes, and a storage tank to store the hot water. Experimental measurements on PV temperature, air and water temperatures on both channels were collected. The PVT performance was evaluated based on the Hottele Whilliere Bliss equation. The controlled indoor operating conditions were solar radiation level of 800 W/m^2, mass flow rates of air and water of 0.05 kg/s and 0.02 kg/s, respectively. It was observed that the achieved electrical and thermal efficiencies were 17 % and 76 %, respectively.

A roll-bond-PVT heat pump with a single-stage compression was experimentally investigated [32]. The designed experimental test contained four pieces of roll-bond-PVT heat pump units, one horsepower (HP) heat pump unit, and 150 liters heat storage tank, which was also integrated with several monitoring sensors to discover the operation characteristics. Therefore, the performance evaluation method was proposed. The investigation by experiments on the system's performance during summer was carried out on electrical and thermal efficiencies. The results of the operating characteristics showed that the system was stable in long term running condition during the daytime. It was shown that the roll-bond-PVT heat pump had a large-scale feasible application value. A model for a PVT heat pump was developed and validated by experiments [33]. The wasted heat was analyzed to improve the performance of the PVT heat pump system. The use of the dual-source PVT heat pump was presented [34]. The proposed formation delivers ground regenera-

tion by cooling the PVT during summer, maintaining the electrical performance near to the maximum power. A suitable disposition of storage tanks allows to decouple the heat sources from the heat pump. On a yearly basis, the proposed design demonstrates to be self-sufficient for the electricity.

PVT heat pump was proposed which consisted of evaporator coils and PV [35]. The PVT heat pump was fabricated with a glass PV. Experimental work was carried out under a typical clear sky condition. Following, the year-round performance of the system was predicted using an already validated numerical model. Results showed that the electrical performance can be improved by 15.20%. In another study, a PVT heat pump performance and the economic aspect of the system were studied (Marco and Renato, 2018). Results showed that primary energy saving was between 35% and 65%, and the investment discounted payback can be around 10 years in mild climates and southern resorts.

A novel design by using a thermal collector of an aluminum material to enhance the heat transfer performance was introduced [36], which was integrated in PVT and PVT-PCM. Experimental measurement validation was carried out for 3-D FEM-based analytical analysis with COMSOL Multiphysics® at solar radiation varying from 200 W/m^2 to 1000 W/m^2 while keeping mass flow rate fixed at a constant value of 0.5 LPM and 32 °C of inlet water temperature. The experiment was conducted in outdoor conditions with passive cooling mode. A good agreement in analytical results and experimental measurements was obtained. PV temperature reduction of 12.6 °C and 10.3 °C is achieved in the case of the PVT-PCM. The highest value of the electrical efficiency achieved was 13.56 % for PV and 13.74% for PVT. Likewise, for PVT-PCM, electrical efficiency was achieved as 13.87 %. In the case of the PVT, the electrical performance was improved to 4.8% and for PVT-PCM, it was improved to 7.6%. Experimental studies on various PVT under different environmental conditions were conducted [36]. Three different systems were used, which contained a convectional PV, water-based-PVT with double absorbing plate, and water-based-PCM. The water-based-PVT had double absorbing plates that were used in which the upper absorbing plate was attached under the PV and the second one was attached to the copper tubes. In water-based-PV/PCM, paraffin wax RT-30 was utilized as the phase change material. The experiment was conducted at three different mass flow rates (0.013, 0.023, and 0.031 kg/s) and their effects on thermal and electrical performances were elaborated. It was concluded that PVT technology could be a significant solution to provide higher thermal and electrical efficiencies.

Studies on the critical mass flow rate is limited in the literature. Adnan *et al*. [37] experimentally studied the optimum $\dot{m}$ that led to the maximum PV efficiency for two PVT designs, namely, the spiral flow and single-pass rectangular tunnel. The critical mass flow rates were 0.011 and 0.0754 kg/s that achieved maximum PV efficiencies of 11 and 10 %, for spiral flow and single-pass rectangular tunnel, respectively. Yazdanifard *et al*. [38] studied the effect of laminar and turbulent flow regimes on the electrical performance of the PVT. There was an optimum $\dot{m}$ which corresponded to the Reynolds number of 2300, and the maximum PV efficiency was 12.5 %. The use of fans to cool the PV was studied by Ameri *et al*. [39]. They used 2, 4, and 8 fans to cool the PV, and concluded that the optimum $\dot{m}$ that can achieve the maximum PV efficiency of 9.5 % was 0.125 kg/s, is when two fans were used.

In previous studies, the critical mass flow rate can be obtained experimentally or theoretically. In either case, the mass flow rate is varied and the corresponding PV efficiency is then obtained by measurement or by theoretical calculations. The trials are repeated until the maximum efficiency is identified by inspection of the values of the efficiencies. As the existing approach is not a time-efficient method, the authors had proposed new equations that can yield the critical mass flow rate directly at any operating conditions [40]. In the present study, we demonstrate further the power of this new method by a case study comparing the critical mass flow rates for two different serpentine designs.

2. PREVIOUS FINDINGS ON NEW EQUATIONS FOR THE CRITICAL MASS FLOW RATES

In this section, the results from the previous study are recapitulated. For the interested reader, the details are available in reference [40]. The symbols used in the equations are explained in the Nomenclature. Better clarification of the symbols is in Ref. [40].

2.1. PV Cell Efficiency Equation

The PV cell efficiency cooled by forced fluid flow, η_{CF}, can be represented as

$$\eta_{CF}=\frac{1}{1-\frac{\eta_{ref}\beta_{ref}\tau_g\beta cI}{U_{tc,a}+U_{tc,p}}\left(1+\frac{U_{tc,p}PF_1}{U_{L2}+F'h_{pf}}+\frac{F'U_{tc,p}h_{pf}PF_1PF_2}{(U_{L2}+F'h_{pf})U_{L,m}}\left[1-\frac{1-\exp\left(-\frac{A_mU_{L,m}\ F'}{\dot{m}C_f}\right)}{\frac{A_mU_{L,m}\ F'}{\dot{m}C_f}}\right]\right)}\left[\eta_{ref}\left[1-\beta_{ref}\left(\left(\frac{\tau_g\beta c\alpha_cI+U_{tc,a}T_a}{U_{tc,a}+U_{tc,p}}+\frac{U_{tc,p}}{U_{tc,a}+U_{tc,p}}\times\right.\right.\right.\right.$$

$$\left.\left.\left.\left.\left[\frac{(\alpha\tau)_{2,eff}I+PF_1\tau_g\alpha_c\beta cI+U_{L2}T_a}{U_{L2}+F'h_{pf}}+\right.\right.\right.\right.$$

$$\left.\left.\left.\left.\frac{F'h_{pf}}{U_{L2}+F'h_{pf}}\left[\left[\frac{PF_2\left(PF_1\tau_g\alpha_c\beta c+(\alpha\tau)_{2,eff}\right)I}{U_{L,m}}+T_a\right]\times\left[1-\frac{1-\exp\left(-\frac{A_mU_{L,m}\ F'}{\dot{m}C_f}\right)}{\frac{A_mU_{L,m}\ F'}{\dot{m}C_f}}\right]+\ T_{in}\left[\frac{1-\exp\left(-\frac{A_mU_{L,m}\ F'}{\dot{m}C_f}\right)}{\frac{A_mU_{L,m}\ F'}{\dot{m}C_f}}\right]\right]\right)-T_{ref}\right)\right]\right]-\frac{P_{Pump}}{I\times A_{PV}},\quad(1)$$

where

$$U_{L2}=\ U_{L1}+U_{tp,a},\tag{1a}$$

and

$$U_{L1}=\frac{U_{tc,p}U_{tc,a}}{U_{tc,a}+U_{tc,p}},\tag{1b}$$

and

$$(\alpha\tau)_{2,eff}=\alpha_p(1-\beta c)\tau_g{}^2.\tag{1c}$$

Defining

$$A=-\frac{\eta_{ref}\beta_{ref}\tau_g\beta cI}{U_{tc,a}+U_{tc,p}},\ B=\frac{U_{tc,p}PF_1}{U_{L2}+F'h_{pf}},C=\frac{F'U_{tc,p}h_{pf}PF_1PF_2}{(U_{L2}+F'h_{pf})U_{L,m}},D=\frac{\tau_g\beta c\alpha_cI+U_{tc,a}T_a}{U_{tc,a}+U_{tc,p}},E=\frac{U_{tc,p}}{U_{tc,a}+U_{tc,p}},$$

$$F=\frac{(\alpha\tau)_{2,eff}I+PF_1\tau_g\alpha_c\beta cI+U_{L2}T_a}{U_{L2}+F'h_{pf}},G=\frac{F'h_{pf}}{U_{L2}+F'h_{pf}},H=\left[\frac{PF_2\left(PF_1\tau_g\alpha_c\beta c+(\alpha\tau)_{2,eff}\right)}{U_{L,m}}+T_a\right],$$

$$X=\left[\frac{1-\exp\left(-\frac{Q}{\dot{m}}\right)}{\frac{Q}{\dot{m}}}\right]\text{ and }\ Q=\frac{A_mU_{L,m}\ F'}{C_f},\text{ Eq. (19) becomes,}$$

$$\eta_{CF}=\frac{1}{1+A[1+B+C[1-X]]}\left[\eta_{ref}\left[1-\beta_{ref}\left(\left(D+\ E\times\left[F+\ G[\ H\times[1-X]+\ T_{in}\ X]\right]\right)-T_{ref}\right)\right]\right]-\frac{P_{Pump}}{I\times A_{PV}}.\tag{2}$$

Rearranging Eq. (2), the expression becomes as,

$$\eta_{CF}=\frac{1}{1+A+AB+AC-ACX}\left[\eta_{ref}[1-\beta_{ref}(D+\ EF+EGH+(EGT_{in}\ -EGH)X-T_{ref})]\right]-\frac{P_{Pump}}{I\times A_{PV}}.\tag{3}$$

Putting $V=D+\ EF+EGH-T_{ref},\ Y=EGT_{in}\ -EGH,W=1+A+AB+AC$ and $R=-AC$ into Eq. (3), the expression becomes

$$\eta_{CF}=\frac{[\eta_{ref}[1-\beta_{ref}(V+YX)]]}{W+RX}-\frac{P_{Pump}}{I\times A_{PV}}.\tag{4}$$

Rearranging Eq. (4), the expression becomes

$$\eta_{CF}=\frac{\eta_{ref}-\eta_{ref}\beta_{ref}V-\eta_{ref}\beta_{ref}YX}{W+RX}-\frac{P_{Pump}}{I\times A_{PV}}.\tag{5}$$

Finally, putting $S=\eta_{ref}-\eta_{ref}\beta_{ref}V,$ and $T=-\eta_{ref}\beta_{ref}Y,$ into Eq. (5), the expression becomes

$$\eta_{CF} = \frac{S+TX\_P_{Pump}}{W+RX\ I\times A_{PV}}. \tag{6}$$

The efficiency of the flow system depends on the flow regime, which depends on the flow rate, or rather the Reynolds number, defined as

$$Re = \frac{\rho v D}{\mu}. \tag{7}$$

For laminar flow, the condition is [41]

$$Re \leq 2300. \tag{8}$$

For transition flow, the condition is [41]

$$2300 < Re \leq 4000. \tag{9}$$

For turbulent flow, the condition is [41]

$$Re > 4000. \tag{10}$$

2.2. Critical Mass Flow Rate for Laminar Flow

If the flow regime in the PVT is established to be in laminar flow, then, following the procedure in Ref. [40], the following equation gives $\dot{m}_c$, the critical mass flow rate:

$$\frac{-T\frac{\exp\left(-\frac{Q}{\dot{m}_c}\right)}{\dot{m}_c}-T\left[\frac{\exp\left(-\frac{Q}{\dot{m}_c}\right)-1}{Q}\right]}{W+R\left[\frac{1-\exp\left(-\frac{Q}{\dot{m}_c}\right)}{\frac{Q}{\dot{m}_c}}\right]}+\frac{S+T\left[\frac{1-\exp\left(-\frac{Q}{\dot{m}_c}\right)}{\frac{Q}{\dot{m}_c}}\right]}{\left(W-R\dot{m}_c\left[\frac{\exp\left(-\frac{Q}{\dot{m}_c}\right)-1}{Q}\right]\right)^2}\times\left(R\frac{\exp\left(-\frac{Q}{\dot{m}_c}\right)}{\dot{m}_c}+R\left[\frac{\exp\left(-\frac{Q}{\dot{m}_c}\right)-1}{Q}\right]\right)-2J\dot{m}_c-3M\dot{m}_c{}^2-N=0, \tag{11}$$

where

$$J=\frac{128\pi\mu L}{\pi^2\rho^2D^4\left(I\times A_{PV}\times\eta_{pump}\right)}, M=\frac{8K}{\pi^2\rho^2D^4\left(I\times A_{PV}\times\eta_{pump}\right)} \text{ and } N=\frac{gL\sin\theta}{\left(I\times A_{PV}\times\eta_{pump}\right)},$$

In Eq. (11), the units of the defined symbols, if any, are given in the Nomenclature.

In reference [40], the solution of Eq. (11) can be further verified to determine whether the $\dot{m}_c$ value so obtained gives a maximum or a minimum point on a $\dot{m}$ versus efficiency plot by using the following Eq. (12).

$$\left.\frac{\partial^2\eta_{CF}}{\partial\dot{m}^2}\right|_{\dot{m}=\dot{m}_{c.Lf}}=\frac{2\times\left[R\left[\frac{\exp\left(-\frac{Q}{\dot{m}}\right)}{\dot{m}}\right]+R\left[\frac{\exp\left(-\frac{Q}{\dot{m}}\right)-1}{Q}\right]\right]^2\left[S-T\dot{m}\left[\frac{\exp\left(-\frac{Q}{\dot{m}}\right)-1}{Q}\right]\right]}{\left[W-R\dot{m}\left[\frac{\exp\left(-\frac{Q}{\dot{m}}\right)-1}{Q}\right]\right]^3}-2\left[R\left[\frac{\exp\left(-\frac{Q}{\dot{m}}\right)}{\dot{m}}\right]+R\left[\frac{\exp\left(-\frac{Q}{\dot{m}}\right)-1}{Q}\right]\right]\times\frac{T\left[\frac{\exp\left(-\frac{Q}{\dot{m}}\right)-1}{Q}+\frac{\exp\left(-\frac{Q}{\dot{m}}\right)}{\dot{m}}\right]}{\left[W-R\dot{m}\left[\frac{\exp\left(-\frac{Q}{\dot{m}}\right)-1}{Q}\right]\right]^2}-$$

$$\frac{QT\exp\left(-\frac{Q}{\dot{m}}\right)}{\dot{m}^3\left[W-R\dot{m}\left[\frac{\exp\left(-\frac{Q}{\dot{m}}\right)-1}{Q}\right]\right]}+\frac{QR\exp\left(-\frac{Q}{\dot{m}}\right)\left[S-T\dot{m}\left[\frac{\exp\left(-\frac{Q}{\dot{m}}\right)-1}{Q}\right]\right]}{\dot{m}^3\left[W-R\dot{m}\left[\frac{\exp\left(-\frac{Q}{\dot{m}}\right)-1}{Q}\right]\right]^2}-2J-6M\dot{m}. \tag{12}$$

2.3. Critical Mass Flow Rate for Transition or Laminar Flow

To find the $\dot{m}_c$ for transition or turbulent flow, the corresponding expression is

$$\frac{-T\frac{\exp\left(-\frac{Q}{\dot{m}}\right)}{\dot{m}}-T\left[\frac{\exp\left(-\frac{Q}{\dot{m}}\right)-1}{Q}\right]}{W+R\left[\frac{1-\exp\left(-\frac{Q}{\dot{m}}\right)}{\frac{Q}{\dot{m}}}\right]}+\frac{S+T\left[\frac{1-\exp\left(-\frac{Q}{\dot{m}}\right)}{\frac{Q}{\dot{m}}}\right]}{\left(W-R\dot{m}\left[\frac{\exp\left(-\frac{Q}{\dot{m}}\right)-1}{Q}\right]\right)^2}\times\left(R\frac{\exp\left(-\frac{Q}{\dot{m}}\right)}{\dot{m}}+R\left[\frac{\exp\left(-\frac{Q}{\dot{m}}\right)-1}{Q}\right]\right)-\frac{3a\dot{m}^2\left[\frac{1.64b}{\log\left[\frac{c}{\dot{m}}+\left(\frac{\varepsilon/D}{3.7}\right)^{1.11}\right]^2}+K\right]}{(I\times A_{PV}\times\eta_{pump})}-$$
$$\frac{3.27abc\dot{m}}{\log\left[\frac{c}{\dot{m}}+\left(\frac{\varepsilon/D}{3.7}\right)^{1.11}\right]^3\left(\frac{c}{\dot{m}}+\left(\frac{\varepsilon/D}{3.7}\right)^{1.11}\right)(I\times A_{PV}\times\eta_{pump})}-\frac{Lg\sin\theta}{(I\times A_{PV}\times\eta_{pump})}=0, \quad (13)$$

where $a=\frac{8}{\pi^2\rho^2D^4}$, $b=\frac{L}{D}$, and $c=\frac{6.9\pi\mu D}{4}$.

Checking the solution of Eq. (13) to see if the $\dot{m}_c$ will give rise to a maximum or minimum efficiency is provided in reference [40] and repeated here as the following:

$$\left.\frac{\partial^2\eta_{CF}}{\partial\dot{m}^2}\right|_{\dot{m}=\dot{m}_{c,Tf}}=\frac{2\times\left[R\left[\frac{\exp\left(-\frac{Q}{\dot{m}}\right)}{\dot{m}}\right]+R\left[\frac{\exp\left(-\frac{Q}{\dot{m}}\right)-1}{Q}\right]\right]^2\left[S-T\dot{m}\left[\frac{\exp\left(-\frac{Q}{\dot{m}}\right)-1}{Q}\right]\right]}{\left[W-R\dot{m}\left[\frac{\exp\left(-\frac{Q}{\dot{m}}\right)-1}{Q}\right]\right]^3}-2\left[R\left[\frac{\exp\left(-\frac{Q}{\dot{m}}\right)}{\dot{m}}\right]+R\left[\frac{\exp\left(-\frac{Q}{\dot{m}}\right)-1}{Q}\right]\right]\times\frac{T\left[\frac{\exp\left(-\frac{Q}{\dot{m}}\right)-1}{Q}+\frac{\exp\left(-\frac{Q}{\dot{m}}\right)}{\dot{m}}\right]}{\left[W-R\dot{m}\left[\frac{\exp\left(-\frac{Q}{\dot{m}}\right)-1}{Q}\right]\right]^2}-$$
$$\frac{QT\exp\left(-\frac{Q}{\dot{m}}\right)}{\dot{m}^3\left[W-R\dot{m}\left[\frac{\exp\left(-\frac{Q}{\dot{m}}\right)-1}{Q}\right]\right]}+\frac{QR\exp\left(-\frac{Q}{\dot{m}}\right)\left[S-T\dot{m}\left[\frac{\exp\left(-\frac{Q}{\dot{m}}\right)-1}{Q}\right]\right]}{\dot{m}^3\left[W-R\dot{m}\left[\frac{\exp\left(-\frac{Q}{\dot{m}}\right)-1}{Q}\right]\right]^2}-\frac{6a\dot{m}\left[K+\frac{1.64b}{\log\left[\frac{c}{\dot{m}}+\left(\frac{\varepsilon/D}{3.7}\right)^{1.11}\right]^2}\right]}{Z}-\frac{13.1abc}{(\dot{m}\times Z)\log\left[\frac{c}{\dot{m}}+\left(\frac{\varepsilon/D}{3.7}\right)^{1.11}\right]^3\left(\frac{c}{\dot{m}}+\left(\frac{\varepsilon/D}{3.7}\right)^{1.11}\right)}-$$
$$\frac{3.27abc^2}{(\dot{m}\times Z)\log\left[\frac{c}{\dot{m}}+\left(\frac{\varepsilon/D}{3.7}\right)^{1.11}\right]^3\left(\frac{c}{\dot{m}}+\left(\frac{\varepsilon/D}{3.7}\right)^{1.11}\right)^2}-\frac{9.81abc^2}{(\dot{m}\times Z)\log\left[\frac{c}{\dot{m}}+\left(\frac{\varepsilon/D}{3.7}\right)^{1.11}\right]^4\left(\frac{c}{\dot{m}}+\left(\frac{\varepsilon/D}{3.7}\right)^{1.11}\right)^2}, \quad (14)$$

where $a=\frac{8}{\pi^2\rho^2D^4}$, $b=\frac{L}{D}$, $c=\frac{6.9\pi\mu D}{4}$, and $Z=I\times A_{PV}\times\eta_{pump}$.

Fig. **2** shows the flowchart for the procedure to obtain the critical mass flow rate.

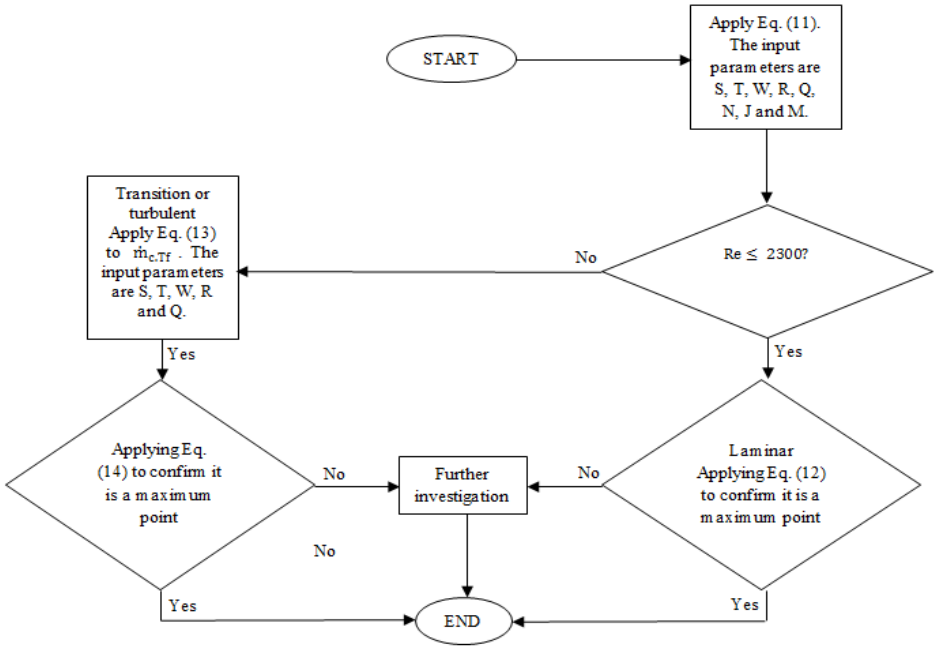

Figure 2: A flowchart for the solution procedure. Modified from Ref. [10].

3. APPLICATION TO A PV COOLER WITH SHEET AND TUBE SERPENTINE DESIGN

In this paper, a 2 mm thick sheet and tube type is used as a PV cooler as shown in Fig. (**3c**). Two different sheet and tube designs with the same area are selected to illustrate the previous mathematical analysis. All tubes are connected in series via 180° flanged return bend with K= 0.2, as shown in Fig. (**3d**). The total numbers of bends for Design A and Design B are 31 and 62, respectively, and the loss coefficient due to the piping fitting are 6.2 and 12.4, respectively. Design A is the example used for illustration in Ref. [40], and Design B is another design for comparison. The comparison of their results will provide further evidence to reinforce the methodology of the new method.

3.1. Design A

Design A contains 32 circular series pipes configuration with outer and inner pipe diameters of 13.3 mm and 12.8 mm, respectively, as illustrated in Fig. (**3a**). The distance between tubes is 25.6 mm.

3.2. Design B

Design B has 64 circular series pipes configuration as shown in Fig. (**3b**). Each tube has outer and inner diameters of 6.9 mm and 6.4 mm, respectively, and the tube spacing is 12.8 mm.

4. RESULTS AND DISCUSSIONS

4.1. The Effect of Mass Flow Rate on the Pumping Requirement

Figure **4** shows the influence of the mass flow rate on the pumping requirements for Design A and Design B. There is a proportional relationship between the mass flow rate and the pumping requirement. The pumping required to push the coolant fluid through the PVT tubes increases as the mass flow rate is increased. For Design A, if the mass flow rate increases from 0 to

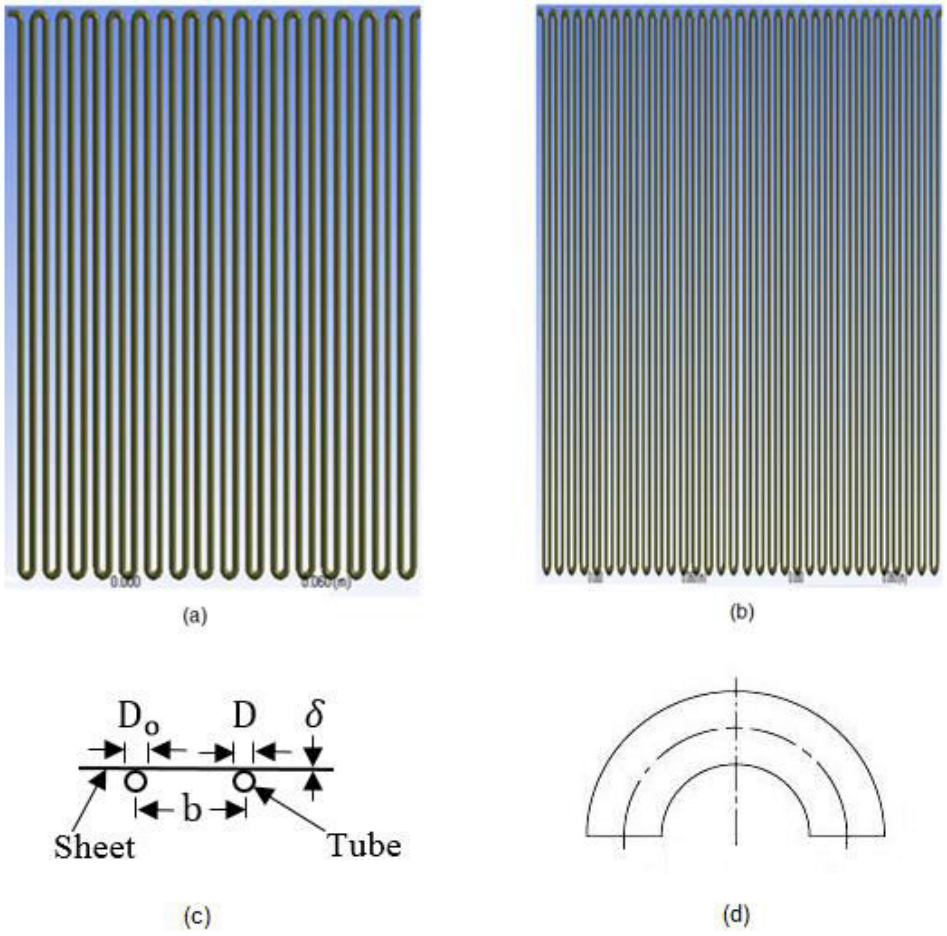

Figure 3: (**a**) Top view of Design A. (**b**) Top view of Design B. (**c**) Section view of sheet and tube type PV cooler. (**d**) 180° flanged return bend with K=0.2.

0.18 kg/s, the pumping requirement will increase from 0 to 26.61 W, while for Design B, the increase is from 0 to 1454 W. It is seen that the pumping requirement for Design B is greater than that of Design A, because of the difference in the collector configuration such as the length, the diameter of the tube and more losses at the pipe fittings.

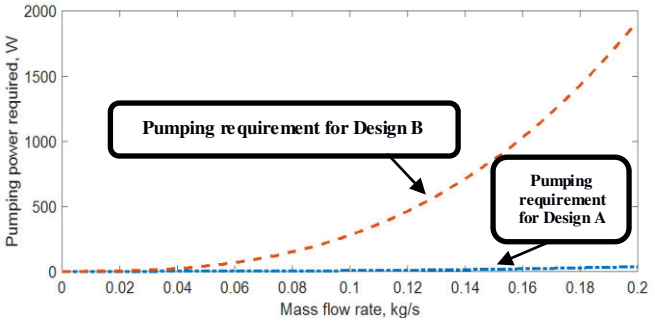

Figure 4: The effect of the mass flow rate on the pumping requirements for Design A and Design B.

4.2. The Effect of Critical Mass Flow Rate on the PV Efficiency for Design A and Design B

Figure **5** shows the effect of the critical mass flow rate on the photovoltaic cell efficiency for Design A. The typical inputs are from Table **1**, and the coefficients (S, T, W, R, Q, N, J, and M) in Eq. (11) can be calculated. Hence, $S = 0.12, T = 0.0246, W = 0.97, R = 0.024, Q = 3.97 \times 10^{-3}$, $N = 0$ and $\theta = 0°$, and they are applied to Eq. (11). The critical mass flow rate, $\dot{m}_c$, that achieves the maximum PV cell efficiency is thus obtained, and it is 0.059 kg/s when $J = 0.08$ and $M = 0.19$. But this critical mass flow rate does not satisfy the condition when $\dot{m}_{c.Lf} < 575\pi\mu D$ (as described in Fig. **2**). The diameter of the pipe is 12.8 mm, and the $\dot{m}_c > 0.023$, implying that the flow is not laminar. Now, applying the direct equation (Eq. (13)), the new critical mass flow rate is 0.041 kg/s which satisfies the condition when $\dot{m}_{c.Tf} > 1000\pi\mu D$, implying that the flow is turbulent. It is a maximum point when Eq. (14) is applied and it gives a value of -2.0785. The maximum PV cell efficiency at 0.041 kg/s is 14.41%. Also shown in Fig. (**5**) is the existing method, where the efficiency needs to be calculated repeatedly over the correct range of mass flow rates before the maximum efficiency can be identified. The broken line shows the expected positions and is seen to yield the same maximum point as the new method).

For Design B (Fig. **6**), $J = 2.53$ and $M = 6.1$, the critical mass flow rate is 0.019 kg/s, and because it does not satisfy the condition $\dot{m}_{c.Lf} < 575\pi\mu D$, the flow is not laminar. Eq. (13) needs to be applied to get the new critical mass flow rate for the transition or turbulent flow regime. The new critical mass flow rate is 0.014 kg/s. This value of mass flow rate indicates that the flow is transition because it satisfied the condition $575\pi\mu D < \dot{m}_{c.Tf} < 1000\pi\mu D$. It is also a maximum point, as applying Eq. (14) yields a value of -0.0151.

Table 1: The PV Cooler Parameters and Operating Conditions for the Two Designs

Parameter	Design A Value	Design B Value
b	0.0256 m	0.0128 m
D	0.0128 m	0.0064 m
Do	0.0133 m	0.0069 m
L	51.2 m	102.4 m
K	6.2	12.4
k	385 W/m K	385 W/m K
n	1	1
α_c	0.85	0.85
α_p	0.83	0.83
A_{PV}	1.31 m^2	1.31 m^2
A_m	1.31 m^2	1.31 m^2
βc	0.83	0.83
β_{ref}	0.0045	0.0045
C_f	4190 J/kg K	4190 J/kg K
ε	0.0015 mm	0.0015 mm
F′	0.9857	0.9857
g	9.8 m/s^2	9.8 m/s^2
h_{pf}	200 W/m^2K	200 W/m^2K
I(t)	1000 W/m^2	1000 W/m^2
μ	1.002×10^{-3} kg/m s	1.002×10^{-3} kg/m s
η_{ref}	0.149	0.149
η_{pump}	75 %	75 %
δ	0.002 m	0.002 m
$P_{out,max}$	195.2 W	195.2 W
ρ	998 kg/m^3	998 kg/m^3
T_a	298 K	298 K
τ_g	0.95	0.95
T_{in}	298 K	298 K
T_{ref}	298 K	298 K
$U_{tc,a}$	9.24 W/m^2K	9.24 W/m^2K
$U_{tc,p}$	332 W/m^2K	332 W/m^2K
θ	0°	0°

This value of critical mass flow rate will correspond to 14.18% maximum PV cell efficiency. It is concluded that the critical mass flow rate is different from one design to another. Again, the broken line shows the expected positions of the trial results using the existing method.

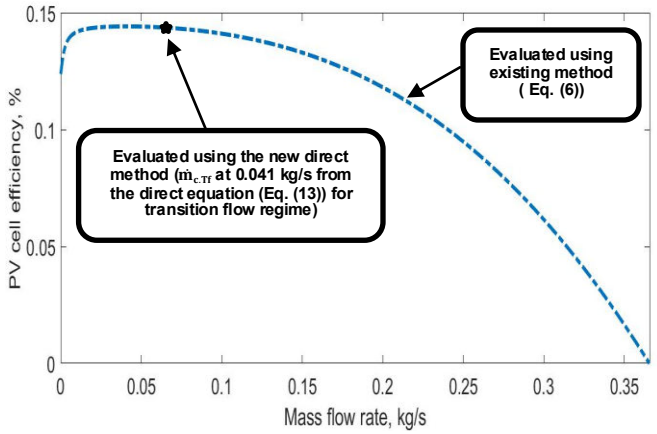

Figure 5: The determination of the critical mass flow rate using the proposed and existing methods for Design A.

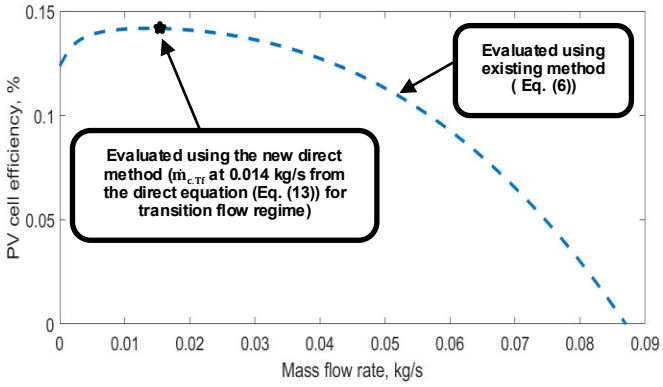

Figure 6: The determination of the critical mass flow rate using the proposed and existing methods for Design B.

Figure **7** shows the percentage of the power consumed by the pump to push the coolant fluid into tubes to the power generated from the PV as the mass flow rate increases for Design A and Design B. It is noticed that the percentage of the ratio for Design A is much lower than that of Design B. This is because of the factors such as the tube's length, diameter, and loss coefficient due to pipe fittings. These parameters will affect the output power from the PV because the pumping requirement will be deducted from the total generated power. From Fig. (7), the values of the ratio are 0.22 % and 1.8 % at mass flow rates of 0.02 kg/s, for Design A and Design B, respectively. If the mass flow rate increases to 0.08, the values of the ratio will increase to 1.5 % and 395 %. At the PV critical mass flow rate, the ratio is 0.22% for Design A while it is 0.18% for Design B. It can be concluded that the pumping power requirement needs to be taken into account when evaluating the PV performance of the PVT.

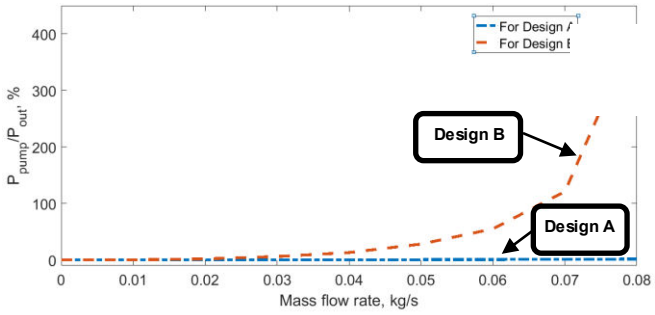

Figure 7: The effects of the mass flow rate on the ratio of the power consumed by the pump to the power generated from the PV for Design A and Design B.

4.3. The Importance of the Critical Mass Flow Rate in the PVT

The importance of evaluating the critical mass flow rate may be summarized as below:

1. Ability to know the maximum PV cell efficiency for the PVT. Therefore, the PV performance comparison between different PVT collector designs will be possible on a level ground.
2. Ability to identify the maximum allowable flow rate without affecting the PV cell efficiency.
3. Ability to distinguish the capability of PVT to cool the PV.
4. The valuation of the pumping cost of the PVT is determined by knowing the maximum allowable flow rate and thus the size of the pump.
5. The use of the critical mass flow rate will be beneficial for researchers and PVT product designers, by knowing the effectiveness of their collector designs for cooling the PV at the early product design stage. For instance, if the PV critical mass flow rate is zero, it means that the collector design is not contributing to cool the PV and thus no improvement on the PV performance can be obtained, urging a re-design.

5. CONCLUSION

In this paper, further analysis on the critical mass flow rate is elaborated via comparing two different sheet and tube designs, namely Design A and Design

B which have different numbers of tubes, tube diameter and length, and pipe fittings. It is shown that the critical mass flow rate is different from one design to another depending on the pipe fitting, geometry of the design, and length and diameter of the tube. Design A and Design B have critical mass flow rates of 0.041 and 0.014 kg/s that correspond to PV efficiencies of 14.41 and 14.18%, respectively, under 1000 W/m^2 of solar radiation along with ambient and inlet water temperatures of 25 ^{o}C. The critical mass flow rate for both designs was elaborated using the direct method that has simplified equations for laminar, transition, and turbulent flow regime. The importance of the critical mass flow was illustrated.

NOMENCLATURE

A	=	area, (m^2)
b	=	tube spacing, (m)
Cf	=	specific heat, (J/kg K)
Cb	=	bond conductance, (W/mK)
D	=	inner diameter of the pipe, (m)
Do	=	outer diameter of the pipe, (m)
f	=	Darcy friction factor
F′	=	flat plate collector efficiency factor
g	=	acceleration due to gravity, (m/s2)
hpf	=	heat transfer coefficient from blackened plate to the water, (W/m^2 K)
I	=	solar intensity, (W/m^2)
J	=	parameter in Eq. (11), (m^2/kg.W)
K	=	loss coefficient
k	=	thermal conductivity of the plate, (W/mk)
L	=	pipe Length, (m)
M	=	parameter in Eq. (11), (m^2/kg.W)
$\dot{m}$	=	mass flow rate, (kg/s)
$\dot{m}_c$	=	critical mass flow rate, (kg/s)
$\dot{m}_{c,Lf}$	=	critical mass flow rate for laminar flow, (kg/s)
$\dot{m}_{c,Tf}$	=	critical mass flow rate for transition/turbulent flow, (kg/s)
N	=	parameter in Eq. (11), (m^2/s2.W)
n	=	number of tubes
P	=	power, (W)
PF1	=	penalty factor due to the glass cover of PV module
PF2	=	penalty factor due to the absorption plate for the portion covered by the PV module
Q	=	parameter in Eq. (11), (W.kg/J.K^2)
q′	=	useful energy gain per unit length, (W/m)
R	=	parameter in Eq. (11)
Re	=	Reynolds number
S	=	parameter in Eq. (11)
T	=	temperature, (°C)
UL,m	=	overall heat transfer coefficient of the PVT, (W/m^2 K)
Utc,a	=	overall heat transfer coefficient from solar cell to the ambient through top surface, (W/m^2 K)
Utc,p	=	overall heat transfer coefficient from back surface of the solar cell to the absorption plate, (W/m^2 K)
Utp,a	=	overall heat transfer coefficient from absorption plate to the ambient, (W/m^2 K)
v	=	velocity of the fluid, (m/s)
W	=	parameter in Eq. (11)

Subscripts

a	=	ambient
c	=	solar cell
eff	=	effective
g	=	glass
m	=	collector
out	=	outlet fluid
max	=	maximum output
P	=	power
Pump	=	water pump
PV	=	photovoltaic
ref	=	reference

Greek Letters

α	=	absorptivity
βc	=	packing factor of solar cell
βref	=	fractional decrease in PV efficiency per unit temperature increase

ε	=	roughness of the copper pipe
μ	=	dynamic viscosity, (kg/ms)
ρ	=	density of the fluid, (kg/m^3)
δ	=	sheet thickness, (m)
η	=	PV cell efficiency
η_{CF}	=	PV cell efficiency cooled by forced convection of fluid
τ	=	transmissivity
θ	=	PVT inclination angle, (°)

REFERENCES

[1] Sultan SM, Tso CP, Ervina EMN. A New Method for Reducing the Performance Evaluation Cost of the Photovoltaic Module Cooling Techniques using the Photovoltaic Efficiency Difference Factor. Case Studies in Thermal Engineering 2020; 100682. https://doi.org/10.1016/j.csite.2020.100682

[2] Sultan SM, Tso CP, Ervina EMN. A New Production Cost Effectiveness Factor for Assessing Photovoltaic Module Cooling Techniques. International Journal of Energy Research 2020; 44: 574-583. https://doi.org/10.1002/er.4889

[3] Sultan SM, Tso CP, Ervina EMN. A New Approach for Photovoltaic Module Cooling Technique Evaluation and Comparison using the Temperature Dependent Photovoltaic Power Ratio. Sustainable Energy Technologies and Assessments 2020; 93: 100705. https://doi.org/10.1016/j.seta.2020.100705

[4] Sultan SM, Tso CP, Ervina EMN. Comments on Performance Evaluation of Photovoltaic Thermal Solar Air Collector for Composite Climate of India. Solar Energy Materials and Solar Cells 2019; 198: 63-64. https://doi.org/10.1016/j.solmat.2019.03.043

[5] Sultan SM, Tso CP, Ervina EMN. A Proposed Temperature-Dependent Photovoltaic Efficiency Difference Factor for Evaluating Photovoltaic Module Cooling Techniques in Natural or Forced Fluid Circulation Mode. Arabian Journal for Science and Engineering 2019; 44: 8123. https://doi.org/10.1007/s13369-019-03932-5

[6] Sultan SM, Tso CP, Ervina EMN. Review on Recent Photovoltaic/Thermal (PV/T) Technology Advances and Applications. Solar Energy 2018; 173: 939-54. https://doi.org/10.1016/j.solener.2018.08.032

[7] Sultan SM, Tso CP, Ervina EMN. A Case Study on Effect of Inclination Angle on Performance of Photovoltaic Solar Thermal Collector in Forced Fluid Mode. Renewable Energy Research and Applications 2019; 173: 187-196.

[8] Garg HP, Agarwal RK. Some Aspects of a PV/T Collector/ Forced Circulation Flat Plate Solar Water Heater with Solar Cells. Energy Conversion and Management 1995; 36(2): 87-99. https://doi.org/10.1016/0196-8904(94)00046-3

[9] David G, Iván A, Montserrat D, Cristina A. Experimental analysis of a novel PV/T panel with PCM and heat pipes. Sustainability, 2020; 12: 1710. https://doi.org/10.3390/su12051710

[10] Mohammad HA, Alireza B, Milad S, Mohammad Z, Amir M, Shahaboddin S, Ravinder K, Mohammad M.. Evaluation of electrical efficiency of photovoltaic thermal solar collector. Engineering Applications of Computational Fluid Mechanics, https://doi.org/10.1080/19942060.2020.1734094

[11] Tao M, Meng L, Arash K.. Photovoltaic thermal module and solar thermal collector connected in series to produce electricity and high-grade heat simultaneously. Applied Energy. 2020; 261: 114380. https://doi.org/10.1016/j.apenergy.2019.114380

[12] Shyam, Tiwari GN, Olivier F, Mishra RK, Al-Helal, IM. Performance evaluation of N-photovoltaic thermal (PVT) water collectors partially covered by photovoltaic module connected in series: An experimental study. Solar Energy. 2016; 134: 302-313. https://doi.org/10.1016/j.solener.2016.05.013

[13] Erkata Y. Methods for the Development and Testing of Polymeric Hybrid Photovoltaic Thermal (PVT) Collector for Indoor Experiments. MethosX. https://doi.org/10.1016/j.mex.2019.10.021

[14] Niccolò, A, Claudio DP, Fabrizio L, Massimiliano M. Performance monitoring and modeling of an uncovered photovoltaic-thermal (PVT) water collector. Solar Energy. 2016; 135: 551-568. https://doi.org/10.1016/j.solener.2016.06.029

[15] Touafek K, Kerrour F. Model Validation of an Empirical Photovoltaic Thermal (PVT) Collector. Energy Procedia. 2014; 74: 1090-1099. https://doi.org/10.1016/j.egypro.2015.07.749

[16] Koronaki IP, Nitsas MT. Experimental and theoretical performance investigation of asymmetric photovoltaic/thermal hybrid solar collectors connected in series. Renewable Energy. 2018; 118: 654-672. https://doi.org/10.1016/j.renene.2017.11.049

[17] Vidya SG, Desh BS, Mishra RK, Sanjeev KS, Tiwari GN. Development of characteristic equations for PVT-CPC active solar distillation system. Desalination. 2018; 445: 266-279. https://doi.org/10.1016/j.desal.2018.08.009

[18] Rohit T, Tiwari GN. Annual performance evaluation (energy and exergy) of fully covered concentrated photovoltaic thermal (PVT) water collector: An experimental validation. Solar Energy. 2017; 146: 180-190. https://doi.org/10.1016/j.solener.2017.02.041

[19] Tiwari GN, Md M, Khan ME. Exergy analysis of N-photovoltaic thermal-compound parabolic concentrator (N-PVT-CPC) collector for constant collection temperature for vapor absorption refrigeration (VAR) system. Solar Energy. 2018; 173: 1032-1042. https://doi.org/10.1016/j.solener.2018.08.031

[20] Evangelos S, Petros A. An experimentally validated, transient model for sheet and tube PVT collector. Solar Energy. 2018; 174: 709-718. https://doi.org/10.1016/j.solener.2018.09.058

[21] Jianhui H, Wujun C, Deqing Y, Bing Z, Hao S, Binbin, G. Energy performance of ETFE cushion roof integrated photovoltaic/thermal system on hot and cold days. Applied Energy. 2016; 173: 40-51. https://doi.org/10.1016/j.apenergy.2016.03.111

[22] Maysam G, Mehran A. Energy and exergy analyses of Photovoltaic/Thermal flat transpired collectors: Experimental and theoretical study. Applied Energy. 2016; 164: 837-856. https://doi.org/10.1016/j.apenergy.2015.12.042

[23] Monia C, Wael C, Hatem M, Philippe, B. Performance evaluation of concentrating solar photovoltaic and photovoltaic/thermal systems. Solar Energy. 2013; 98: 315-321. https://doi.org/10.1016/j.solener.2013.09.029

[24] Proell M, Karrer H, Brabec CJ, Hauer A. The influence of CPC reflectors on the electrical incidence angle modifier of c-Si cells in a PVT hybrid collector. Solar Energy. 2016; 126: 220-230. https://doi.org/10.1016/j.solener.2016.01.012

[25] Bernardo LR, Perers B, Hakansson H, Karlsson B. Performance evaluation of low concentrating

photovoltaic/thermal systems: A case study from Sweden. Solar Energy. 2011; 85: 1499-1510. https://doi.org/10.1016/j.solener.2011.04.006

[26] Kunnemeyer R, Anderson TN, Duke M, Carson JK. Performance of a V-trough photovoltaic/thermal concentrator. Solar Energy. 2014; 101: 19-27. https://doi.org/10.1016/j.solener.2013.11.024

[27] Chaoqing F, Hongfei Z, Rui W, Xinglong M. Performance investigation of a concentrating photovoltaic/thermal system with transmissive Fresnel solar concentrator. Energy Conversion and Management. 2016; 111: 401-408. https://doi.org/10.1016/j.enconman.2015.12.086

[28] Chemisana D, Rosell JI, Riverola A, Lamnatou C. Experimental performance of a Fresnel-transmission PVT concentrator for building-façade integration. Renewable Energy. 2016; 85: 564-572. https://doi.org/10.1016/j.renene.2015.07.009

[29] Milad M, Reza H. A photovoltaic/thermal system with a combination of a booster diffuse reflector and vacuum tube for generation of electricity and hot water Production. Renewable Energy. 2015; 78: 245-252. https://doi.org/10.1016/j.renene.2015.01.010

[30] Othman MY, Hamid SA, Tabook MAS, Sopian K, Roslan M, Ibarahim HZ. Performance analysis of PVT Combi with water and air heating system: An experimental study. Renewable Energy. 2016; 86: 716-722. https://doi.org/10.1016/j.renene.2015.08.061

[31] Wei P, Yanan C, Qian Z, Hongwen Y, Xiaoyan Z, Yongzhe Z, Hui Y. Comparative investigation of performances for HIT-PV and PVT systems. Solar Energy. 2019; 179: 37-47. https://doi.org/10.1016/j.solener.2018.12.056

[32] Franz H, Christian H, Franz I, Peter K. System efficiency of pvt collector-driven heat pumps. International Journal of Thermofluids 2020; 5-6: 100034. https://doi.org/10.1016/j.ijft.2020.100034

[33] Renato L, Marco N. Photovoltaic/thermal (PV/T)/ground dual source heat pump: Optimum energy and economic sizing based on performance analysis. Energy & Buildings. 2020; 211: 109800. https://doi.org/10.1016/j.enbuild.2020.109800

[34] Vaishak S, Purnanand VB. Performance analysis of a heat pump-based photovoltaic/thermal (PV/T) system. Clean Technologies and Environmental Policy. 2020. https://doi.org/10.1007/s10098-020-01839-6

[35] Fayaz H, Rahim NA, Hasanuzzaman M, Rivai A, Nasrin R. Numerical and outdoor real time experimental investigation of performance of PCM based PVT system. Solar Energy. 2019; 179: 135-150. https://doi.org/10.1016/j.solener.2018.12.057

[36] Sajan P, Brij B, Tarun M. Experimental investigation of water based photovoltaic/thermal (PVT) system with and without phase change material (PCM). Solar Energy. 2017; 155: 1104-1120. https://doi.org/10.1016/j.solener.2017.07.040

[37] Ibrahim A, Jin GL, Daghigh R, Salleh MHM, Othman MY, Ruslan MH, Mat S and Sopian K, Hybrid Photovoltaic Thermal (PV/T) Air and Water Based Solar Collectors Suitable for Building Integrated Applications. American Journal of Environmental Sciences 2009; 5(5): 618-624. https://doi.org/10.3844/ajessp.2009.618.624

[38] Yazdanifard F, Ebrahimnia-Bajestan E, Ameri M. Investigating the performance of a water-based photovoltaic/thermal (PV/T) collector in laminar and turbulent flow regime. Renew. Energy. 2016; 99: 295-306. https://doi.org/10.1016/j.renene.2016.07.004

[39] Ameri M, Mahmodabadi MM, Shahsavar A. An experimental study on a photovoltaic/thermal (PV/T) air collector with direct coupling of fans and panels Energy Sources. 2012; 34: 929-947. https://doi.org/10.1080/15567031003735238

[40] Sultan SM, Tso CP, Ervina EMN. Alternative determination of critical mass flow rate for the photovoltaic solar thermal collector in forced fluid mode. Case Studies in Thermal Engineering. 2021; 23: 100805. https://doi.org/10.1016/j.csite.2020.100805

[41] Cengel, Y. A., and Cimbala, J. Fluid and Mechanics fundamentals and applications. Mc Graw Hill. 2006.

Received on 18-12-2020 Accepted on 30-12-2020 Published on 31-12-2020

DOI: https://doi.org/10.15377/2409-5826.2020.07.7